

Yes, multi-periodic dwarfs in Upper Scorpius are binaries

ANDREI TOKOVININ¹ AND CESAR BRICEÑO¹

¹*Cerro Tololo Inter-American Observatory, Casilla 603, La Serena, Chile*

ABSTRACT

We found that multi-periodic low-mass stars discovered by *Kepler* K2 in the Upper Scorpius association are close binaries with typical separations of the order of 10 au and large mass ratios. These stars were surveyed by speckle interferometry at the SOAR telescope with spatial resolution of 0".04. Out of 129 observed targets, we resolved 70 pairs (including 16 previously known ones and three new triple systems). The distribution of projected separations of binaries with primary stars less massive than the Sun corresponds to a log-normal with median of 11.6 au and logarithmic dispersion of 0.60 dex, similar to M dwarfs in the field. Future orbits of newly discovered binaries will provide accurate measurements of masses to calibrate pre-main sequence evolutionary tracks; a tentative orbit of one previously known binary is determined here.

1. INTRODUCTION

As stars condense from gas, the excess of angular momentum is removed by a combination of mechanisms. Rotation and multiplicity of young stars reflect the result of this complex, still poorly understood process where disks play a major role. This is the context of the present work.

The *Kepler* K2 campaigns furnished massive amounts of high-quality photometry of several young stellar clusters and associations, bringing statistical studies of stellar rotation to a new level. [Rebull et al. \(2018\)](#) (hereafter RSC18) found that about 20% of low-mass stars in the Pleiades and Praesepe clusters and in the Upper Scorpius (USco) association have two or more photometric periods. They interpreted this as different rotation periods of comparable-brightness components in unresolved binaries. The location of multi-periodic stars on the color-magnitude diagrams (CMDs) supports this interpretation. However, [Rebull et al.](#) note that multiple periods can result from other phenomena such as differential rotation; they believe that low-mass multi-periodic stars are predominantly binaries, while some multi-periodic stars of higher mass are not binary. On the other hand, a binary with a large magnitude difference or an inactive component may have only one photometric period. So, not all binaries are multi-periodic and not all multi-periodic stars are binary.

Identification of most low-mass multi-periodic stars with binaries still lacks a direct proof. Moreover, the separations of those hypothetical binaries remain unknown. Binary separation impacts the size and survival of the circumstellar disks which influence the rotation. [Stauffer et al. \(2018\)](#) determined that young low-mass multi-periodic stars rotate, on average, faster than single-stars, and related this finding to the different disk properties in single and multiple stars.

We observed 129 multi-periodic stars in USco from Table 1 of RSC18 by speckle interferometry and spatially resolved 70 of them. This supports the proposed interpretation of low-mass multi-periodic stars as being mostly binaries and provides the distribution of their separations. Most resolved binaries have components of similar brightness, but we cannot tell to what extent this reflects the distribution of the mass ratios because our sample favors near-equal binaries.

The observations are presented in Section 2, their results are given in Section 3 and are discussed in Section 4.

2. OBSERVATIONS

2.1. Instrument and data

We used the high-resolution camera (HRCam) on the 4.1 m Southern Astrophysical Research Telescope (SOAR) located at Cerro Pachón in Chile. The detector in HRCam has been recently replaced by a better camera, gaining at least one magnitude in sensitivity. The instrument, observing procedure, and data reduction are covered in ([Tokovinin 2018](#)); see recent results and references in ([Tokovinin et al. 2018](#)).

atokovinin@ctio.noao.edu

Corresponding author: Andrei Tokovinin

This project did not have regular time allocation at SOAR. However, we observed these targets on 2018 April 2 for two hours while working with HRCam on another project. Our goal was to evaluate quickly the feasibility of this study. Surprisingly, we could cover 52 targets and resolved 2/3 of them. This provided a strong stimulus to continue. Another two hours were devoted to this work on 2018 May 26, enlarging the observed sample. The third and last observing run on 2018 June 25 used two hours of engineering time.

The alt-azimuth mount of SOAR prevents observations close to the zenith. So, the USco region (declination $\sim -25^\circ$) was observed before the meridian, on the Eastern side. On April 2, the seeing was excellent, the vibrations inherent to the SOAR telescope were absent, and we obtained good data on the 52 brightest targets with $V < 15.5$ mag. As these observations were exploratory, we took for each target only two data cubes: one with the standard 200×200 pixel ($3''.15$ size) format and 50 ms exposure time, another with the extended 400×400 pixel size, 2×2 detector binning, and a longer exposure of 100 ms. This second data cube would detect fainter companions at separations up to $3''$ (which are rare in this sample). All data were taken with the I filter (824/170 nm bandwidth).

On 2018 May 26, the seeing was not so good. We pursued the project by observing 32 targets down to $V = 16$ mag. Fainter magnitudes and worse seeing degraded the sensitivity, and we had to use the long exposure time of 50 ms and the 2×2 binning. For each target, two 200×200 (narrow-field) data cubes were taken, so we could miss companions wider than $1''.5$. The resolution was somewhat worse than on the first night, so we could have also missed some close pairs.

The last observing run on June 25 had an average seeing. We took data in the standard mode (without binning) for targets brighter than $I = 12$ mag and with 2×2 binning for fainter ones. In this run, we extended the program to multi-periodic stars with $I < 10$ mag from RSC18, thus hoping to enlarge the number of pre-main sequence (PMS) binaries suitable for future orbit determination and measurement of masses.

The data cubes were processed in the standard way (Tokovinin 2018) by calculating the power spectra and the associated speckle auto-correlation functions (ACFs). The shift-and-add images centered on the brightest pixel in each frame are produced as well. However, they are useful only for determination of the true quadrant for brighter targets, when the companion is detectable in such images and the magnitude difference exceeds 0.5 mag. Parameters of each resolved binary (position angle, separation, and magnitude difference)

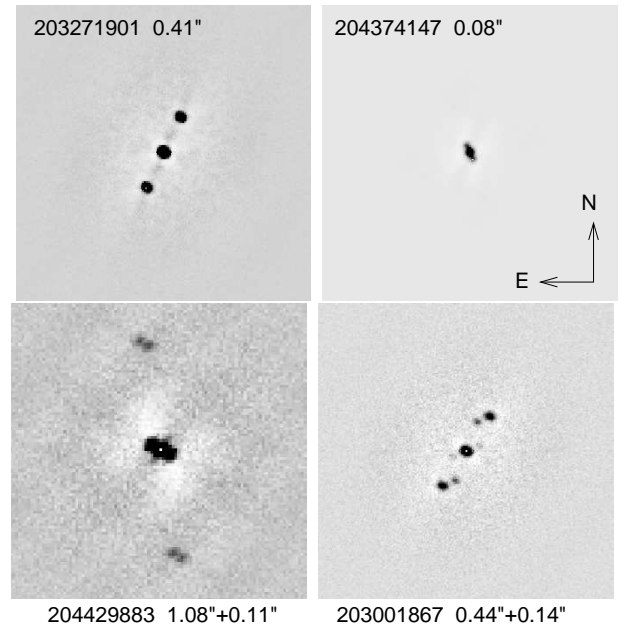


Figure 1. Speckle auto-correlation functions of two newly resolved binaries (top) and two new triples (bottom), in negative rendering. The frame size is $3''.15$, North is up and East left. The EPIC numbers and separations are indicated.

are determined by fitting a model to the power spectrum. The pixel scale ($0''.01575$) and detector orientation are accurately measured on a set of calibration binaries for each observing run.

Figure 1 gives examples of the ACFs for two resolved binaries and two newly discovered triple systems.

2.2. Observed sample

Table 1 of RSC18 contains 239 multi-periodic stars in USco. The sensitivity of HRCam allowed us to observe only the brightest part of this sample with $I < 13$ mag and $(V - K)_0 < 6$ mag, corresponding to spectral types earlier than M5V, approximately. Figure 2 shows the $(M_V, V - K)$ CMD for the observed targets. We used the *Gaia* DR2 (Gaia collaboration 2018) parallaxes (replaced by the average parallax of 7.04 mas if not available) and applied individual de-reddening corrections from RSC18. The full line is a 8 Myr isochrone for solar metallicity from Bressan et al. (2012), also used by Rebull et al. As all these stars are deemed to be binaries, they should be displaced from the isochrone upwards by as much as 0.75 mag (dashed line). On average, the observed stars are located 0.5 mag above the isochrone, with an rms scatter of 0.7 mag.

The masses of main components were estimated from the de-reddened absolute V magnitudes by assuming the average shift of +0.75 mag above the 8 Myr isochrone. Considering the slope of the isochrone and the scatter, the errors of the estimated masses are $\sim 0.1 M_\odot$. Al-

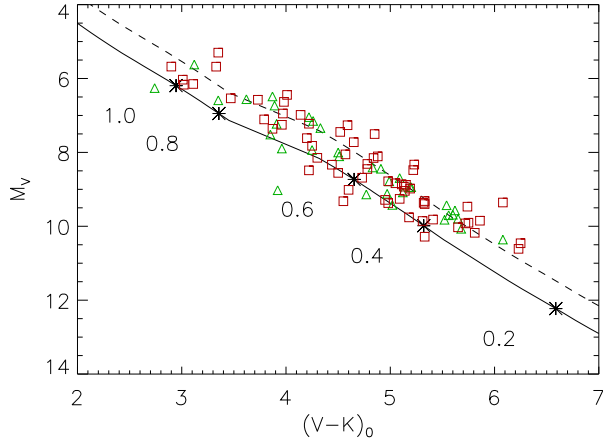


Figure 2. Color-magnitude diagram for the sample of multi-periodic dwarfs in USco observed here (absolute V magnitude vs. de-reddened color $(V - K)_0$). Red squares mark the resolved binaries, green triangles are unresolved stars. The full line is the 8 Myr isochrone for solar metallicity from [Bressan et al. \(2012\)](#) (asterisks and numbers indicate masses), the dashed line shifts it up by 0.75 mag.

though these masses depend on the model isochrones and assumed age and hence could be biased, they are useful for relative ranking of our objects in mass. The masses range from 0.25 to $3 \mathcal{M}_\odot$; the median mass is $0.63 \mathcal{M}_\odot$. The colors $(V - K)_0 > 3$ mag correspond to spectral types later than K5V, but these PMS stars will have somewhat earlier spectral types when they arrive on the main sequence.

Table 1. The observed sample

EPIC	α	δ	I_C	$V - K$	$\bar{\omega}$	ρ	ΔI	Mass	Note ^a
	J2000		(mag)	(mag)	(mas)	($''$)	(mag)	(\mathcal{M}_\odot)	
204562176	15 55 2.13	-21 49 43.4	10.62	3.82	6.17	0.95	
204175508	15 55 17.58	-23 22 3.7	7.92	1.04	8.24	1.63	W?,4
203553934	15 55 29.81	-25 44 49.9	11.47	4.79	...	0.37	0.2	0.59	D?
203710077	15 55 48.81	-25 12 24.0	9.52	2.21	6.95	1.45	
204918279	15 56 25.09	-20 16 16.2	12.60	6.67	...	0.18	0.2	0.29	
204104740	15 56 27.62	-23 38 52.1	11.55	5.19	7.14	0.16	0.1	0.56	
204832936	15 56 42.43	-20 39 34.2	12.86	5.74	7.00	1.41	3.2	0.38	D,G
204248842	15 57 3.67	-23 04 48.6	12.83	5.93	6.46	0.32	
203696502	15 57 15.56	-25 15 13.3	7.99	0.87	6.20	0.20	2.0	1.73	W
203628765	15 57 16.74	-25 29 19.3	10.84	3.81	...	0.58	0.1	0.82	W,D?
204179058	15 57 34.31	-23 21 12.3	11.27	4.63	6.93	0.05	0.6	0.74	W,G+,4
204780592	15 58 30.39	-20 53 35.9	6.85	0.73	7.04	2.06	
204066898	15 58 36.21	-23 48 2.1	12.70	5.47	8.17	0.37	
204281210	15 58 36.92	-22 57 15.3	8.70	3.04	6.02	1.52	D
203301463	15 59 11.89	-26 35 0.8	7.58	1.16	7.18	0.66	1.8	1.77	
204477741	15 59 18.38	-22 10 43.2	12.74	6.19	6.77	0.05	0.0	0.31	
203462615	15 59 38.05	-26 03 23.6	12.93	6.24	7.72	0.25	
203499724	15 59 49.88	-25 55 58.8	12.01	5.04	6.29	0.59	
204436170	15 59 59.95	-22 20 36.7	10.90	4.62	7.15	0.72	W
204878974	16 00 31.35	-20 27 5.0	11.16	4.79	11.04	0.14	0.4	0.56	W
204350593	16 00 41.34	-22 40 41.8	12.16	5.50	7.40	0.11	0.1	0.42	
203363279	16 00 42.65	-26 23 29.6	8.60	1.60	6.39	1.61	3
204406748	16 01 5.18	-22 27 31.1	11.14	4.99	...	0.28	0.6	0.69	W
204428324	16 01 10.36	-22 22 27.9	12.39	5.98	6.87	0.36	
203690414	16 01 13.97	-25 16 28.4	12.95	5.54	...	0.18	0.4	0.32	D
204794876	16 01 47.43	-20 49 45.7	10.87	4.58	6.89	0.06	0.6	0.73	W
204246759	16 03 33.79	-23 05 19.0	10.88	3.44	6.30	0.93	

Table 1 continued

Table 1 (*continued*)

EPIC	α	δ	I_C	$V - K$	$\bar{\omega}$	ρ	ΔI	Mass	Note ^a
	J2000		(mag)	(mag)	(mas)	($''$)	(mag)	(\mathcal{M}_\odot)	
204862109	16 03 54.96	-20 31 38.5	10.88	4.58	6.60	0.09	0.2	0.73	W
203895983	16 04 18.93	-24 30 39.3	11.23	4.96	...	0.29	0.1	0.74	D
204637622	16 04 20.98	-21 30 41.6	11.99	5.68	6.79	0.06	0.0	0.50	D,d?
204603210	16 04 35.87	-21 39 22.3	12.42	5.68	7.29	0.09	0.6	0.39	G+
204856827	16 06 59.37	-20 33 4.7	12.13	5.80	7.32	0.07	0.0	0.44	
204844509	16 07 3.56	-20 36 26.4	10.20	4.13	...	0.21	0.4	0.78	W
204506777	16 07 17.78	-22 03 36.5	7.99	1.70	6.87	1.67	
204242152	16 07 23.75	-23 06 24.1	12.33	5.32	6.33	0.07	0.0	0.45	
204757338	16 07 27.46	-20 59 44.4	12.94	6.48	...	0.57	0.0	0.30	D
204845955	16 07 44.48	-20 36 3.2	11.66	5.74	6.77	0.06	0.4	0.53	W,3
204229583	16 07 57.76	-23 09 23.6	11.54	5.23	7.29	2.40	1.0	0.55	G,3
203851147	16 07 58.76	-24 41 31.9	12.37	5.57	...	0.64	0.6	0.38	
205087483	16 08 1.55	-19 27 58.2	12.23	5.59	...	0.84	0.0	0.46	W,G
203271901	16 08 4.10	-26 40 44.9	11.32	4.59	...	0.41	0.4	0.71	
203788687	16 08 5.22	-24 55 33.2	8.42	1.79	6.75	0.94	2.8	1.63	W
205080616	16 08 23.24	-19 30 0.9	11.79	4.76	7.25	0.60	D
205141287	16 08 34.36	-19 11 56.2	9.81	3.95	...	0.31	1.1	1.03	3
204810792	16 08 35.14	-20 45 29.6	7.60	1.67	7.89	1.68	
204099739	16 08 39.08	-23 40 5.6	11.63	5.33	6.92	0.56	
205177770	16 08 43.07	-19 00 52.1	12.91	6.05	...	0.15	0.6	0.30	
204852312	16 08 54.07	-20 34 18.4	12.69	6.33	7.06	0.34	
202724025	16 08 56.94	-28 35 57.7	12.19	5.67	6.85	0.70	
204429883	16 09 20.62	-22 22 5.9	12.20	6.40	...	0.12	0.0	0.38	W,T,G,4
205203376	16 09 29.19	-18 52 53.7	10.56	4.36	10.63	0.22	1.6	0.69	
204608292	16 09 35.74	-21 38 5.9	12.38	5.29	11.00	0.12	1.3	0.36	
204059992	16 10 1.83	-23 49 43.5	12.72	5.79	7.10	0.58	
203036995	16 10 3.09	-27 28 39.8	12.39	5.62	...	0.12	0.7	0.38	
204060981	16 10 56.18	-23 49 29.2	12.06	5.80	6.84	0.47	
203716047	16 10 57.91	-25 11 10.3	12.43	5.40	...	0.46	0.6	0.39	
203754361	16 11 7.43	-25 03 1.8	12.12	5.43	6.18	0.49	
204217530	16 11 15.95	-23 12 14.6	8.43	1.24	6.46	1.60	D,4
205168266	16 12 5.99	-19 03 44.3	7.44	1.19	7.19	2.13	
204857023	16 12 8.24	-20 33 1.6	12.46	5.94	7.05	1.80	0.6	0.54	
203760219	16 13 2.34	-25 01 46.0	11.69	4.57	7.12	0.07	0.2	0.69	
205373716	16 13 20.80	-17 57 52.1	12.47	5.83	6.99	0.35	
205373893	16 13 21.23	-17 57 49.1	12.61	5.67	7.37	0.40	
203048597	16 13 24.56	-27 26 13.4	12.31	5.52	...	0.74	0.0	0.39	G
204156820	16 13 36.44	-23 26 27.0	11.74	5.14	...	0.55	0.0	0.59	
205225696	16 13 43.50	-18 45 52.8	13.26	6.64	...	0.21	0.0	0.34	
204459941	16 13 43.66	-22 14 59.4	11.20	4.10	6.27	0.06	0.4	0.73	
203917770	16 13 45.49	-24 25 19.5	6.14	0.35	5.98	1.74	3.0	2.97	W,G,3
202947197	16 13 47.81	-27 47 33.9	8.69	1.28	6.57	0.36	4.5	1.54	T,D?,4
203777800	16 13 56.62	-24 57 56.9	12.65	5.42	...	0.20	0.1	0.39	
203799762	16 14 3.79	-24 53 9.1	12.29	4.60	6.48	0.60	
204449800	16 14 10.10	-22 17 23.7	12.58	6.91	6.46	0.84	0.0	0.31	G
205047378	16 14 13.81	-19 39 36.2	8.56	2.36	6.28	1.55	
204488355	16 14 20.50	-22 08 9.7	7.28	0.84	7.25	1.78	4
205188906	16 14 28.92	-18 57 22.5	11.92	5.23	7.08	0.51	D
204235325	16 14 52.68	-23 08 2.7	12.11	5.44	7.13	0.70	1.2	0.44	
202533810	16 15 0.60	-29 19 34.8	11.80	4.91	...	0.17	0.0	0.52	
204204606	16 15 54.86	-23 15 14.9	12.86	5.52	...	0.27	0.0	0.33	
203433962	16 16 17.20	-26 09 10.2	10.96	4.51	6.50	0.72	
204082531	16 16 20.10	-23 44 14.4	12.78	5.81	7.91	0.06	0.0	0.27	

Table 1 *continued*

Table 1 (*continued*)

EPIC	α	δ	I_C	$V - K$	$\bar{\omega}$	ρ	ΔI	Mass	Note ^a
	J2000		(mag)	(mag)	(mas)	($''$)	(mag)	(\mathcal{M}_\odot)	
203750949	16 16 22.94	-25 03 46.7	7.84	1.17	6.48	1.77	
203771564	16 16 25.17	-24 59 19.4	7.47	0.91	6.37	2.31	W?
203703588	16 16 44.25	-25 13 45.3	8.32	1.15	6.85	1.65	4
203855509	16 16 47.93	-24 40 28.4	12.93	6.18	6.35	0.07	0.4	0.35	3
203809634	16 17 26.14	-24 50 59.4	12.49	6.02	6.58	0.43	
203809317	16 17 29.94	-24 51 3.2	12.36	5.71	...	0.41	0.5	0.52	
205267399	16 18 41.87	-18 32 40.1	12.65	5.70	8.67	0.29	
204569229	16 19 45.38	-21 47 57.7	11.27	4.38	7.54	0.05	0.4	0.66	
204655550	16 20 27.24	-21 26 6.8	11.41	4.45	7.78	0.08	0.9	0.63	
204666965	16 20 36.40	-21 23 12.3	12.62	5.86	7.39	0.31	
203891936	16 20 44.68	-24 31 38.3	10.54	3.89	6.09	0.76	
204372172	16 20 50.23	-22 35 38.7	8.44	1.24	6.95	1.65	D
204494885	16 21 21.14	-22 06 32.2	8.02	1.22	6.29	1.75	
204471912	16 21 41.26	-22 12 5.7	12.55	5.91	7.53	0.33	
203495721	16 21 47.92	-25 56 47.1	8.75	1.34	7.62	1.47	
204603511	16 22 10.05	-21 39 17.3	8.15	1.00	7.19	1.65	D,3
202800875	16 22 13.14	-28 18 58.5	11.21	4.14	6.30	0.72	
203517602	16 22 22.30	-25 52 20.2	12.07	6.00	6.99	0.51	
204374147	16 22 34.21	-22 35 12.3	11.05	5.46	6.97	0.08	0.9	0.71	3
204591415	16 22 44.06	-21 42 22.4	12.44	5.78	6.63	0.43	
202908892	16 22 51.57	-27 55 37.4	12.63	5.22	6.83	0.39	
203001867	16 23 59.01	-27 36 3.7	11.91	5.34	...	0.44	0.3	0.53	T
203649927	16 24 2.89	-25 24 53.9	8.20	2.70	5.82	2.62	D,G+
203783190	16 24 6.33	-24 56 46.9	10.58	4.71	...	0.24	0.2	0.94	
203761347	16 24 21.31	-25 01 31.4	7.42	2.21	7.15	2.71	4.6	2.70	W,G,4
204355491	16 24 51.36	-22 39 32.5	8.58	2.73	7.22	0.04	0.5	1.57	W
204462113	16 24 55.33	-22 14 28.6	12.69	5.30	7.91	0.08	0.2	0.40	
203888630	16 25 7.32	-24 32 27.2	11.95	6.51	...	0.29	0.0	0.84	4
203911473	16 25 19.24	-24 26 52.7	9.05	2.26	7.45	0.14	0.0	1.57	W
203071614	16 25 55.40	-27 21 24.4	12.55	5.72	8.06	0.11	0.4	0.29	
203476597	16 25 57.91	-26 00 37.3	10.79	4.58	6.32	0.77	
203086979	16 26 2.15	-27 18 14.1	11.02	3.79	7.47	0.73	
203881373	16 26 9.31	-24 34 12.1	9.01	5.45	7.06	2.88	D
203937317	16 26 17.07	-24 20 22.0	10.72	6.15	7.45	0.93	D
204611221	16 26 19.61	-21 37 21.0	11.84	5.13	7.53	0.55	
204520585	16 26 41.19	-22 00 9.7	11.75	5.06	5.90	0.11	0.9	0.70	
203856244	16 26 41.22	-24 40 17.7	12.11	7.95	5.96	0.14	0.5	0.44	W,D
203442191	16 27 6.68	-26 07 31.1	9.46	2.11	6.14	1.57	
203850605	16 27 19.49	-24 41 40.3	10.76	4.87	8.90	0.15	0.0	0.60	W,D
203115615	16 28 45.14	-27 12 19.5	12.36	5.59	4.55	0.13	1.0	0.65	
202615424	16 29 11.39	-29 00 31.7	12.34	5.00	...	0.13	0.0	0.52	
203873374	16 29 35.09	-24 36 10.7	12.50	8.84	...	0.19	0.1	0.48	D
204559470	16 33 38.82	-21 50 26.3	11.38	5.47	6.78	0.71	
203181641	16 34 5.85	-26 58 44.2	10.67	3.60	7.32	0.09	1.1	0.87	
202679988	16 35 11.88	-28 45 52.0	10.93	3.72	6.67	0.06	0.9	0.84	
205059490	16 36 39.22	-19 36 7.5	8.82	1.32	6.24	1.61	4
203135082	16 36 52.88	-27 08 18.6	9.23	2.04	6.21	1.47	
205075874	16 38 28.57	-19 31 26.0	9.31	1.83	5.03	1.64	
205002311	16 47 47.33	-19 52 31.9	8.47	1.26	8.46	1.48	D

^aNotes: W – listed in WDS; D – disk or possible disk in RSC18; G – companion measured in Gaia; G+ – additional Gaia companion; T – triple; 3,4 – three or 4 periods.

Table 1 lists the 129 observed stars, identified by their EPIC numbers in column (1) and J2000 coordinates in

columns (2) and (3). In columns (4) and (5) we give the I_C magnitude and the $(V - K)$ color (without reddening correction), as determined by RSC18. Column (6) contains the *Gaia* DR2 (Gaia collaboration 2018) parallaxes, where available. The separations and magnitude differences of resolved pairs are listed in columns (7) and (8), respectively. Column (8) gives the primary mass estimated from the isochrone. The notes in column (9) are explained below.

We matched the targets to the *Gaia* DR2 within $6''$ radius to get their parallaxes. These are missing only for 28 stars. All these 28 stars are binaries with separations from $0''.11$ to $0''.84$, where the resolved nature of the source was apparently detected by *Gaia* and prevented parallax measurement. Closer binaries are unresolved by *Gaia* and treated there as single stars, while components of wider binaries have separate entries in DR2, allowing us to compute their relative positions and magnitude differences. *Gaia* measured nine pairs wider than $0''.8$, also measured here. The agreement between *Gaia* and HRcam astrometry of common pairs is very good. Three targets (EPIC 204179058, 204603210, 203649927) have additional *Gaia* companions with matching parallaxes and proper motions (marked G+ in Table 1) at separations of $3''.76$, $5''.52$, and $2''.06$, respectively. The first two stars also have close companions, so these systems are in fact triple. These additional *Gaia* companions are faint and fall outside the $4''$ *Kepler* pixels, explaining why only double periods were detected for these stars by RSC18. The first one, EPIC 204179058, is flagged by RSC18 as potentially disk-bearing. EPIC 204248842 has a *Gaia* source at $1''.2$ separation with a large magnitude difference of $\Delta G = 5.1$ mag and unknown parallax; we have not detected this companion with HRcam and consider it optical or spurious. Finally, two objects (EPIC 204878974 and 20408292) have parallaxes of 11 mas, challenging their membership in USco; however, both are $0''.1$ binaries unresolved by *Gaia*, hence these parallaxes are likely biased. The *Gaia* astrometry confirms membership of all our targets in the USco association.

The sample was created regardless of known binaries listed in the Washington Double Star Catalog, WDS (Mason et al. 2001). In fact, 16 resolved targets are previously known binaries (marked by W in the notes). One previously known binary from this sample was not detected by us, being too close (EPIC 204436170, WDS J16000–2221, KSA 122, $0''.025$); two more (EPIC 204175508 = J15553–2322 = KOH 25 and 203771564 = J16164–2459 = KOU 59) with separations on the order of $1''$ are not confirmed either by us or by *Gaia*, being apparently spurious (marked W?). Overall, we resolved

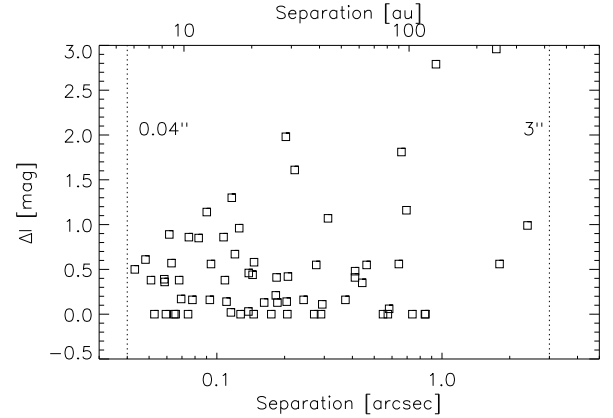


Figure 3. Magnitude difference ΔI vs. angular separation for resolved binaries. The upper axis assumes distance of 140 pc for converting angular separations to au. Vertical dotted lines delimit the surveyed range of separations.

57 new pairs (counting each subsystem in triples separately); the total number of resolved pairs in our sample stands at 70. The other symbols in the notes are T – triple, D or D? – star with disk according to RSC18, 3 or 4 – number of periods detected, if more than two.

Figure 3 plots magnitude difference ΔI vs. separation to characterize the limits of our observations. Small separations and moderate ΔI dominate, with a sharp cutoff below the resolution limit of $0''.04$. The plot hints that there are many even closer, unresolved binaries in our sample. On the other hand, only 4 pairs out of 70 have separations above $1''.5$, exceeding the maximum detectable separation in the narrow-field data cubes. All these (and wider) companions are also resolved by *Gaia*, so our survey is not impaired by the narrow field size. Moreover, the vast majority of pairs are closer than $1''.5$.

3. RESULTS

3.1. Astrometry

Table 2 gives measurements of resolved pairs. Its first column has the WDS-style code based on the J2000 coordinates. For previously known pairs, their WDS discoverer codes are given in column (2), while column (3) gives the EPIC numbers. Then follow the date of observation (4), position angle (5), and the measurement error in tangential direction σ_θ in mas (6). Columns (7) and (8) give the separation and its error, respectively. The last column (9) gives ΔI to within 0.1 mag, which is the minimum error of differential speckle photometry. The flags in this column mean noisy data (:), alternative photometry of wider pairs (*), and quadrant identification (q).

For nine resolved pairs, *Gaia* DR2 astrometry gives relative positions and magnitude differences in the G

band (flag G in Table 1). We include those data in Table 2, with the epoch of 2015.5 and the flag G in the last column. The *Gaia* results give independent test of our measurements. We also include positions of three wide G+ physical companions with discovery code 'Gaia'.

Table 2. Measurements of resolved pairs

WDS	Discoverer	EPIC	Epoch	θ	σ_θ	ρ	$\sigma\rho$	ΔI
(2000)	Designation		+2000	(deg)	(mas)	($''$)	(mas)	(mag)
15555–2545	...	203553934	18.2524	137.4	0.3	0.3725	0.3	0.2
15564–2016	...	204918279	18.3999	173.7	6.1	0.1827	3.5	0.2 :
			18.4846	177.3	1.6	0.1695	2.2	0.0 :
15565–2339	...	204104740	18.2524	102.2	0.2	0.1623	0.3	0.1
15567–2040	...	204832936	18.4846	38.9	8.0	1.4086	8.0	3.2 *
			15.5000	39.3	...	1.407	...	3.2 G
15573–2515	B 301	203696502	18.4817	256.0	0.6	0.2025	0.2	2.0 q
15573–2529	KOH 57 AB	203628765	18.2523	143.5	0.2	0.5826	0.4	0.1
			18.3999	143.7	0.6	0.5832	0.9	0.1
15576–2321	KSA 119 AB	204179058	18.2524	87.2	1.4	0.0482	2.3	0.6
	Gaia AC		15.5000	350.9	...	3.760	...	6.1 G
15592–2635	...	203301463	18.4817	191.9	0.3	0.6608	0.2	1.8 *
			18.4817	192.0	0.8	0.6626	1.2	3.1
15593–2211	...	204477741	18.4846	84.2	18.9	0.0528	18.9	0.0 :
16001–2027	KOH 63	204878974	18.2526	134.6	1.5	0.1441	1.8	0.4
16007–2241	...	204350593	18.4847	56.6	1.4	0.1104	2.7	0.1 :
16011–2228	KOH 65	204406748	18.2526	339.7	0.1	0.2764	0.6	0.6 q
16012–2516	...	203690414	18.3999	50.7	9.3	0.1842	3.6	0.4 :
16018–2050	KOH 67	204794876	18.2526	358.8	3.6	0.0629	2.2	0.6
16039–2032	KOH 70 AB	204862109	18.2526	91.0	1.4	0.0931	3.5	0.2
			18.3999	93.9	1.7	0.0968	0.6	0.1 :
16043–2131	KOH 71	204637622	18.2526	139.4	0.3	0.0647	3.5	0.0 :
16043–2431	...	203895983	18.4846	67.2	0.4	0.2940	0.5	0.1
16046–2139	AB	204603210	18.3999	131.7	1.1	0.0942	1.6	0.6 :
	Gaia AC		15.5000	93.7	...	5.527	...	1.6 G
16070–2033	...	204856827	18.2526	120.7	0.3	0.0656	0.3	0.0 :
16071–2036	KSA 125 Aa,Ab	204844509	18.2526	339.8	0.5	0.2069	0.6	0.4 q
16074–2306	...	204242152	18.2526	13.1	1.7	0.0745	1.4	0.0 :
16075–2060	...	204757338	18.4847	112.5	1.7	0.5749	1.1	0.0 :
16077–2036	BOY 20	204845955	18.2526	57.8	0.3	0.0584	0.3	0.4 :
16080–1928	LAF 114	205087483	18.4847	313.8	0.5	0.8443	0.5	0.0
			15.5000	314.0	...	0.845	...	0.1 G
16080–2309	...	204229583	18.2524	35.8	0.1	2.3983	0.1	1.0 :
			15.5000	35.9	...	2.388	...	1.0 G
16080–2442	...	203851147	18.3999	228.7	1.1	0.6432	1.1	0.6 :
16081–2456	DON 781	203788987	18.4818	338.7	1.1	0.9404	0.6	2.8 *
16081–2641	...	203271901	18.2524	154.0	0.2	0.4107	0.5	0.4
16086–1912	...	205141287	18.4847	143.0	0.6	0.3117	0.4	1.1 q
16087–1901	...	205177770	18.4847	141.1	1.1	0.1463	8.8	0.6 :
16093–2222	WSI 130 Aa,Ab	204429883	18.3999	61.2	4.9	0.1155	0.9	0.0 :
			15.3354	51.0	...	0.126	...	0.2
16093–2222	WSI 130 Aa,B	204429883	18.3999	187.3	4.5	1.0843	6.8	1.8 :
			15.3354	190.2	...	1.1458	...	2.2 q

Table 2 continued

Table 2 (continued)

WDS	Discoverer	EPIC	Epoch	θ	σ_θ	ρ	σ_ρ	ΔI
(2000)	Designation		+2000	(deg)	(mas)	($''$)	(mas)	(mag)
			15.5000	189.5	...	1.121	...	2.1 G
16095–1853	...	205203376	18.2526	166.2	2.5	0.2217	2.2	1.6 q
16096–2138	...	204608292	18.2526	131.0	3.7	0.1165	1.0	1.3 q
16101–2729	...	203036995	18.2524	156.6	1.6	0.1203	3.4	0.7
16110–2511	...	203716047	18.2524	71.5	1.4	0.4626	0.4	0.5 :
			18.4846	71.5	1.0	0.4624	1.1	0.2 :
16121–2033	...	204857023	18.4847	129.5	0.4	1.8017	0.4	0.6 *
			15.5000	129.8	...	1.792	...	0.6 G
16130–2502	...	203760219	18.2524	152.0	0.9	0.0694	2.0	0.2
16134–2726	...	203048597	18.2524	147.2	0.3	0.7388	0.3	0.0
			15.5000	145.6	...	0.741	...	0.1 G
16136–2326	...	204156820	18.2524	155.9	0.3	0.5471	0.7	0.0
			18.4847	155.7	0.8	0.5482	0.8	0.0 :
16137–1846	...	205225696	18.4847	63.4	2.8	0.2056	16.8	0.0 :
16137–2215	...	204459941	18.2526	110.6	0.2	0.0586	0.2	0.4 :
16138–2425	B 307 AB	203917770	18.4818	217.4	0.4	1.7434	0.5	3.0 *
			15.5000	218.0	...	1.729	...	3.4 G
16138–2748	AB	202947197	18.4817	271.4	0.9	0.3618	0.5	4.5
16138–2748	BC	202947197	18.4817	195.3	0.5	0.0630	2.4	0.7
16139–2458	...	203777800	18.3999	23.6	6.0	0.2043	2.3	0.1 :
16142–2217	...	204449800	18.4847	35.6	1.5	0.8400	1.5	0.0 :
			15.5000	35.4	...	0.838	...	0.0 G
16149–2308	...	204235325	18.2524	39.6	0.6	0.6951	0.9	1.2 *
16150–2920	...	202533810	18.2524	61.3	0.2	0.1745	1.4	0.0
16159–2315	...	204204606	18.3999	95.7	1.8	0.2707	5.5	0.0 :
16163–2344	...	204082531	18.3999	21.1	12.7	0.0594	13.8	0.0 :
16175–2451	...	203809317	18.4846	308.8	2.5	0.4112	1.1	0.5 :
16198–2148	...	204569229	18.2526	95.9	0.3	0.0510	0.3	0.4 :
16205–2126	...	204655550	18.4847	37.5	3.3	0.0751	9.5	0.9 :
16226–2235	...	204374147	18.2526	204.3	2.2	0.0830	1.3	0.8 q
16240–2525	Gaia	203649927	15.5000	8.4	...	2.059	...	4.1 G
16240–2736	AB	203001867	18.2524	145.9	0.0	0.4424	0.8	0.4 :
			18.3999	146.6	0.1	0.4370	0.2	0.3 :
16240–2736	BC	203001867	18.2524	293.0	5.2	0.1403	2.7	1.0 :
			18.3999	291.8	0.2	0.1469	0.2	0.8 :
16241–2457	...	203783190	18.2524	67.7	0.3	0.2429	0.1	0.2
16244–2502	B 308 AB	203761347	18.4818	142.2	1.2	2.7129	1.2	4.6 *
			15.5000	142.2	...	2.704	...	4.4 G
16249–2214	...	204462113	18.2526	156.2	0.5	0.0779	0.5	0.2 :
16249–2240	KSA 129 Aa,Ab	204355491	18.4818	331.7	0.9	0.0432	1.6	0.5
16251–2432	...	203888630	18.4846	103.3	2.4	0.2902	4.3	0.0 :
16253–2427	B 309	203911473	18.4818	295.9	0.5	0.1381	0.7	0.0
16259–2721	...	203071614	18.3999	159.4	3.1	0.1086	4.7	0.4 :
16267–2200	...	204520585	18.2526	231.9	1.3	0.1071	6.8	0.9 q
16267–2440	RAT 7	203856244	18.4846	78.0	4.8	0.1386	5.0	0.5 :
16273–2442	CST 8 AB	203850605	18.2524	77.8	0.3	0.1457	1.5	0.0
16282–2451	...	203810698	18.4846	101.2	3.7	3.6236	2.7	1.0 :
16288–2712	...	203115615	18.3999	149.7	1.7	0.1257	1.2	1.0 :
16292–2901	...	202615424	18.3999	144.5	6.1	0.1275	2.5	0.0 :
16296–2436	...	203873374	18.4846	129.2	7.8	0.1858	69.2	0.1 :
16341–2659	...	203181641	18.4846	243.4	4.5	0.0902	5.7	1.1 q
16352–2846	...	202679988	18.4846	63.7	0.3	0.0615	5.0	0.9

3.2. Distribution of separations

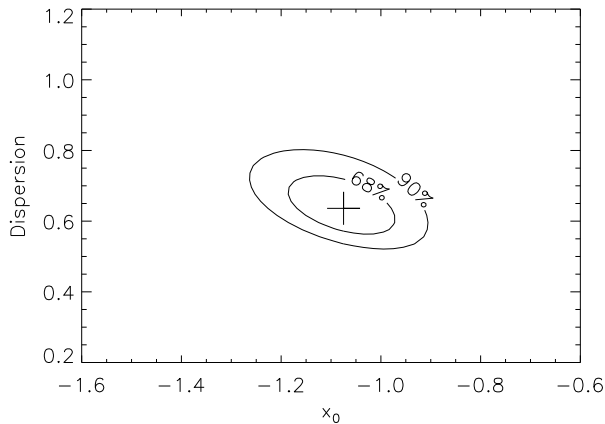


Figure 4. Contours of the likelihood function for objects with masses $< 1M_{\odot}$ in the (x_0, σ) plane that correspond to the significance levels of 68% and 90%.

Distribution of periods or separations of low-mass binaries is frequently approximated by a log-normal function. Let $x = \log_{10} \rho$ be the decimal logarithm of the separation ρ . The log-normal distribution $f(x)$,

$$f(x) = \epsilon(2\pi\sigma)^{-1} \exp[-(x - x_0)^2/(2\sigma^2)], \quad (1)$$

has three parameters: multiplicity fraction ϵ , median separation x_0 , and the logarithmic dispersion σ . These parameters were determined by the maximum likelihood (ML) method (see for example the Appendix of Tokovinin 2014). We assume the detection probability that rises linearly in the separation range from $0''.04$ to $0''.07$ (inspired by the sharpness of the cutoff in Figure. 3) and equals one for separations $\rho < 3''$ (binaries with larger separations are ignored). For stars with several companions, we use the smallest separation from the primary component (separation between A and B in triple systems like A-BC and AB-C). The derived separation distribution characterizes all companions regardless of magnitude difference ΔI . As tight pairs with large ΔI can be missed (see Figure 3), the distribution can be biased to larger separations.

The first parameter, multiplicity fraction, is naturally restricted to the range $0 < \epsilon < 1$. The ML fitting leads to $\epsilon = 1$ (i.e. all targets are binary). The two remaining free parameters, x_0 and σ , are slightly correlated, as shown in Figure 4.

The results of parameter-fitting for sub-samples in selected ranges of mass are given in Table 3. Its first column gives the mass range, the second column is the median mass in this range. Then follow the total number of observed targets and the number of resolved binaries (ignoring pairs with $\rho > 3''$). The remaining columns give the best-fit parameters x_0 and σ and their formal errors corresponding to 68% confidence intervals (“ 1σ ”). Fig-

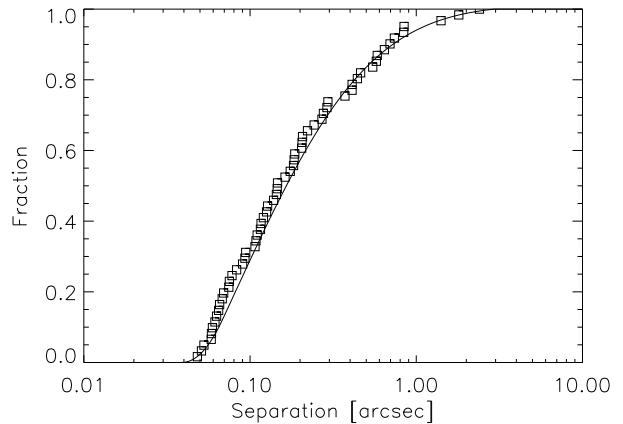


Figure 5. Cumulative distribution of projected separations (squares) and its log-normal model (line) for 95 binaries less massive than $1M_{\odot}$.

Table 3. Separation distribution

Range	$\langle M \rangle$	N_{tot}	N_{bin}	x_0	σ	ϵ
(M_{\odot})	(M_{\odot})				(dex)	
< 1	0.52	95	61	$-1.08^{+0.09}_{-0.09}$	$0.64^{+0.08}_{-0.06}$	> 0.91
< 0.5	0.38	44	29	$-1.04^{+0.14}_{-0.13}$	$0.62^{+0.13}_{-0.08}$	> 0.85
$0.5-1$	0.69	51	32	$-1.11^{+0.13}_{-0.12}$	$0.65^{+0.12}_{-0.08}$	> 0.87
> 1	1.65	34	9
All	0.63	129	70	$-1.20^{+0.11}_{-0.11}$	$0.79^{+0.11}_{-0.08}$	> 0.91

ure 5 shows the cumulative distribution of projected separations for the $< 1M_{\odot}$ sub-sample and its ML model. At the smallest separations, the distribution is shaped by the detection limit (note the initial quadratic rise). The log-normal model fits the data quite well.

We see that the log-normal distributions approximating the full sample and its sub-groups are mutually consistent, showing robustness of the result. The raw fraction of resolved binaries is always close to $2/3$ and the derived multiplicity fraction is always $\epsilon = 1$ (the 68% confidence lower limits of ϵ are given in Table 3). Only massive targets with $M > 1M_{\odot}$ stand apart by the low fraction of resolved binaries, 0.26. The ML fitting for this group does not yield meaningful parameters owing to the small number of binaries. We do not discuss these stars further and focus only on 95 targets with $M < 1M_{\odot}$.

Assuming the distance of 140 pc, the median separation is 11.6 au ($x_0 = 1.07$ au). The logarithmic dispersion is 0.6 dex. Both parameters do not vary significantly between the low- and high-mass parts of the sample. We caution that the formal errors of the log-

normal parameters are meaningful only when the true distribution is indeed log-normal.

Let us compare the log-normal separation distribution found here with prior knowledge on the statistics of low-mass binaries. Janson et al. (2012) surveyed early M-type dwarfs in the solar neighborhood and found that their semimajor axes match the log-normal distribution with $x_0 = 1.2$ au and $\sigma = 0.8$ dex. This team also observed dwarfs of spectral types later than M5V in the field (Janson et al. 2014) and derived the more compact distribution shifted to smaller separations: $x_0 = 0.78$ au and $\sigma = 0.47$ dex. On the other hand, solar-mass binaries in the field have a larger median separation $x_0 = 1.7$ au and a larger dispersion $\sigma = 1.32$ dex (Tokovinin 2014).

The multi-periodic stars in USco observed here have separation distribution similar to that of field M dwarfs. However, the trend of decreasing median separation and dispersion with decreasing mass, observed in the field, is not found in this sample; the distribution of binary separations in USco appears to be independent of mass in the range from 0.3 to $1 M_\odot$.

3.3. New triple stars

The lower panels of Figure 1 illustrate new triple systems discovered in this program. The first one, EPIC 20429883, is listed in WDS as J16093–2222 or WSI 130, but only as a $1''$ binary. Its discovery in 2010 was announced recently by Mason et al. (2018). We detected the inner close pair Aa,Ab composed of two equal stars, while the previously known distant companion B is substantially fainter, hence less massive. Interestingly, RSC18 found 4 distinct photometric periods for this star. It was observed at SOAR in 2015.3, but the triple nature was overlooked at the time. We include the 2015 measures in Table 2. The inner pair Aa,Ab turned by 10° in 3 years.

Another triple star EPIC 202947197 (J16138–2748) was discovered in June. A $0''.06$ pair of faint stars B and C is located at $0''.36$ from the main star A, which has a relatively large mass of $1.5 M_\odot$. RSC18 suspected a disk and detected 4 photometric periods.

The third triple system EPIC 203111867 (J16240–2736) is a new discovery made in April and confirmed by re-observation in May. Here, the close $0''.14$ pair B,C orbits the central star A at $0''.44$. Note that the ratio of separations is small, only 3.1. So, this young triple system could be dynamically unstable, unless comparable separations result from projection on the sky and the real ratio is larger. RSC18 detected only two periods.

Our sample contains at least two unresolved compact triple systems. One of those, EPIC 204506077

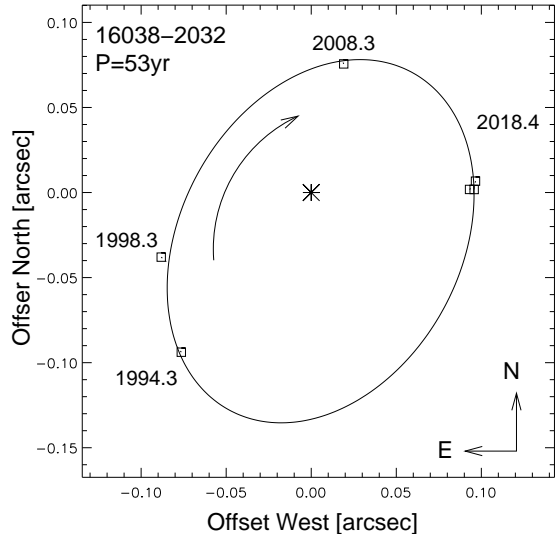


Figure 6. Preliminary orbit of EPIC 204862109 (WDS J16038-2032, KOH 70) with a period of 53 years. Squares with dates denote measurements of the secondary companion relative to the primary, placed at the coordinate origin.

(HD 144548), is a triply eclipsing system with periods of 33.9 and 1.63 day (Alonso et al. 2015). The directly measured mass of the primary star, $1.44 M_\odot$, compares well with $1.67 M_\odot$ estimated here from the isochrone. Another triple is EPIC 203476597, where David et al. (2016) found a 1.4 day eclipsing binary accompanied by a more massive star. For both triples, RSC18 detected only two photometric periods.

There are triple systems with outer companions outside the survey radius of $3''$ listed in the WDS (EPIC 204844509 and 203937317) and three new triple systems with wide companions found by *Gaia* (EPIC 204179058, 204637622, and 204649937). For several other objects in Table 1, RSC18 found three or four distinct photometric periods that could be produced by additional stars in the systems.

3.4. Orbits and masses

With a separation of 10 au and a mass sum of $1 M_\odot$, the orbital period of a typical binary is around 30 years. We note that the positions of some previously known close binaries re-discovered here differ from the published measures, owing to their orbital motion. One of the brightest pairs in our sample, EPIC 204862109 (WDS J16038-2032, KOH 70), has 3 prior measures dating back to 1994 and shows considerable orbital motion. Combining these data with our own measures, we computed a tentative orbit shown in Figure 6. Its elements are: $P = 52.6$ year, $T_0 = 2006.3$, $e = 0.3$, $a = 0''.116$, $\Omega = 147^\circ 6$, $\omega = 127^\circ 5$, and $i = 136^\circ 4$. Us-

ing the DR2 parallax of 6.59 ± 0.22 mas, we compute the mass sum of $1.7 M_{\odot}$. Considering potential bias of the DR2 parallax (its large error is likely caused by binarity) and the intrinsic uncertainty of masses derived from the isochrones, the estimated mass sum of $1.5 M_{\odot}$ matches quite well the mass derived from the orbit.

Further monitoring of the orbital motion and a better parallax measurement from forthcoming *Gaia* data releases will result in accurate masses that will help to calibrate evolutionary tracks of young stars. We expect that future *Gaia* data releases will detect acceleration of these stars (including closer binaries that are not resolved here). New close pairs discovered here are amenable to orbit determination if their motion is monitored in the future.

4. DISCUSSION

The large number of newly resolved binaries appears somewhat surprising, considering that USco has received considerable attention from this perspective. The pioneering work by Koehler et al. (2000) surveyed 118 stars in USco with an angular resolution of $0''.13$ and revealed many binaries (hence the discoverer codes KOH in WDS). Kraus & Hillenbrand (2007) used seeing-limited 2MASS imagery (see also the follow-up work by Aller et al. 2013). Kraus et al. (2008) explored USco stars brighter than $R = 14$ mag and north of -25° with high-contrast aperture masking, excluding known binaries, while Kraus & Hillenbrand (2012) used laser adaptive optics to probe binarity of the 78 lowest-mass members of USco. Janson et al. (2013) and Lafrenière et al. (2014) observed members of USco not covered by previous high-resolution imaging.

These high-resolution studies involved modest samples and did not cover the complete USco association. As most low-mass stars are single, a sample of ~ 100 targets yields only ~ 20 binaries. In contrast, we start here with multi-periodic stars selected from the large parent sample. Our targets are from the outset expected to be binaries with components of comparable flux. This pre-selection ensures the large fraction of resolved binaries we found. With only a few hours of telescope time, we could substantially enlarge the number of known binaries among low-mass members of USco. Many new tight pairs have short periods and are an excellent material for future calibration of PMS stellar evolutionary models.

It will be interesting to test binarity of unresolved multi-periodic targets using either a higher spatial resolution and/or a high-resolution spectroscopy. Both approaches involve large telescopes, hence pre-selection of unresolved targets from this study would be a valuable starting point allowing to save telescope time. We expect that *Gaia* will resolve many of these stars, will detect their accelerations, and will determine astrometric orbits of the closest and fastest pairs. Lunar occultations is another potentially interesting method of probing binarity in USco, although it is applicable only to relatively bright stars.

We are grateful to J. Stauffer who suggested to look at multi-periodic stars using speckle interferometry and made valuable comments on the early versions of this paper. This work used the SIMBAD service operated by Centre des Données Stellaires (Strasbourg, France), bibliographic references from the Astrophysics Data System maintained by SAO/NASA, and the Washington Double Star Catalog maintained at USNO.

Facilities: SOAR

REFERENCES

- Aller, K. M., Kraus, A. L., Liu, M. C. et al. 2013, *ApJ*, 773, 63
- Alonso, R., Deeg, H. J., Hoyer, S., et al. 2015 *A&A*, 584, L8
- Bressan, A., Marigo, P., Girardi, L. et al. 2012, *MNRAS*, 427, 127
- David, T. J., Hillenbrand, L. A., Cody, A. M. et al. 2016, *ApJ*, 816, 21
- Gaia* Collaboration, Brown, A. G. A., Vallenari, A., Prusti, T. et al. 2018, *A&A*, in preparation (Vizier Catalog I/345/gaia2).
- Janson, M., Hormuth, F., Bergfors, C. et al. 2012, *ApJ*, 754, 44
- Janson, M., Lafrenière, D., Jayawardhana, R. et al. 2013, *ApJ*, 773, 170
- Janson, M., Bergfors, C., Brandner, W. et al. 2014, *ApJ*, 789, 102
- Koehler, R., Kunkel, M., Leinert, C. & Zinnecker, H. 2000, *A&A*, 356, 541
- Kraus, A. L., Ireland, M. J., Martinache, F. & Lloyd, J. P. 2008, *ApJ*, 679, 762
- Kraus, A. L. & Hillenbrand, L. A. 2007, *ApJ*, 662, 413
- Kraus, A. L. & Hillenbrand, L. A. 2012, *ApJ*, 757, 141
- Lafrenière, D., Jayawardhana, R., van Kerkwijk, M. H. et al. 2014, *ApJ*, 785, 47

Mason, B. D., Wycoff, G. L., Hartkopf, W. I., Douglass, G. G. & Worley, C. E. 2001, AJ, 122, 3466 (WDS)
Mason, B. D., Hartkopf, W. I., Miles, K. N. et al. 2018, AJ, 155, 215
Rebull, L. M., Stauffer, J. R., Cody, A. M. et al. 2018, AJ, 155, 196 (RSC18)
Stauffer, J. R., Rebull, L. M., Cody, A. M. et al. 2018, ApJ, submitted

Tokovinin, A. 2014, AJ, 147, 87

Tokovinin, A. 2018, PASP, 130, 5002

Tokovinin, A., Mason, B. D., Hartkopf, W. I. et al. 2018, AJ, 155, 235